

Oceanic and Atmospheric Drivers of Post-El-Niño Chlorophyll Rebound in the Equatorial Pacific



¹ Hyung-Gyu Lim, ²John P. Dunne, ²Charles A. Stock, ²Paul Ginoux, ^{2,3}Jasmin G. John, and ²John Krasting

¹AOS program, Princeton University, ²NOAA/OAR/Geophysical Fluid Dynamics Laboratory, Princeton, NJ, USA

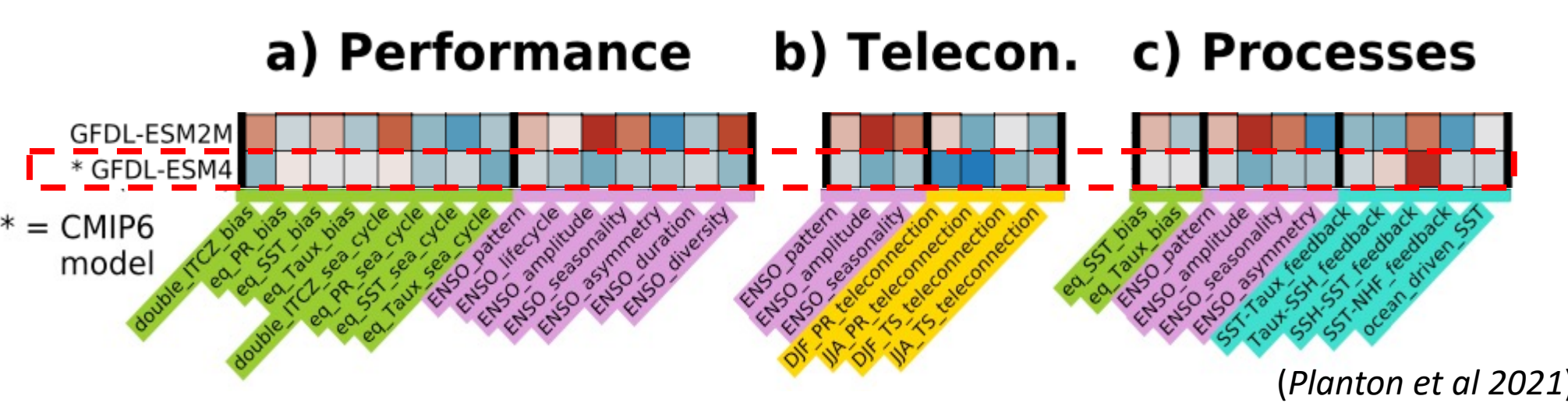
³NOAA/OAR/Atlantic Oceanographic and Meteorological Laboratory, Miami, FL, USA

Motivation

✓ New generation GFDL-ESM4.1 (Dunne et al 2020; Stock et al 2020)

➢ Better fidelity of ENSO simulation (Planton et al 2021)

➢ Dynamic dust-iron deposition in land to ocean delivery (Evans et al 2016)



Q) GFDL-ESM4.1 do better ENSO-CHL coupling?

Evaluating dominant factor whether physical driven or iron cycling driven?

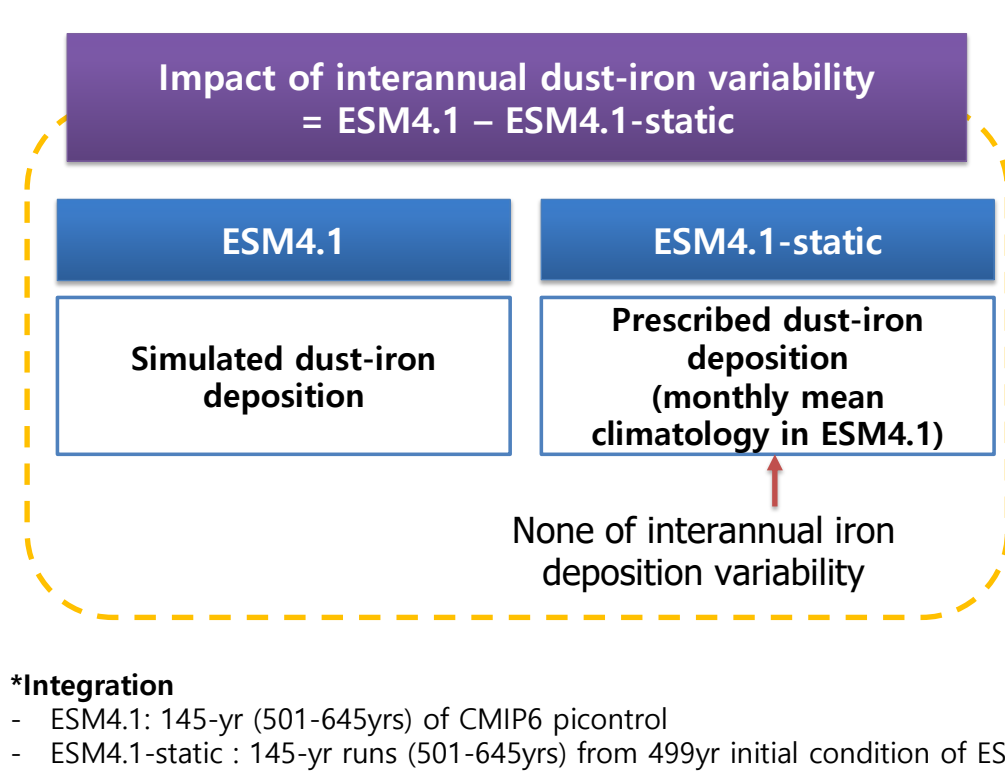
Datasets

- piControl simulations from two generations of GFDL earth system models: years 1001–1100 of ESM2M; years 501–645 of ESM4.1
- Satellite-derived ocean color for chlorophyll estimation: the European Space Agency Ocean Colour Climate Change Initiative project (ESA-CCI) version 4.2
- NOAA Extended Reconstructed SST version 5 (ERSST v5).
- Vertical temperature profiles: version 3.4.2 of the Simple Ocean Data Assimilation (SODA)
- Two satellite-derived aerosol optical thicknesses: NOAA Climate Data Record (CDR) of AVHRR Daily and Monthly Aerosol Optical Thickness (AOT) over Global Oceans, Version 3.0; SeaWiFS Deep Blue Level 3 monthly product which contains monthly global gridded ($1^\circ \times 1^\circ$) data derived from SeaWiFS Deep Blue Level 3 daily gridded data (Hsu et al., 2013).

Methods

- ✓ Linear regression for variables against November to January (NDJ) averaged SST anomalies (SSTa) in the Niño3.4 region ($170^\circ - 120^\circ$ W, 5° N– 5° S; Niño3.4 SSTa) (Trenberth, 1997) is employed to diagnose general ENSO influences.
- ✓ Converted to 1degree horizontal resolution
- ✓ Observation for September 1997 until December 2018
- ✓ Linear trends and seasonal cycles were removed from all data sets.
- ✓ All data sets are smoothed using a 3-month running mean to focus on the seasonal ENSO-chlorophyll evolution and its variability.

ESM4.1-static run



**Oceanic Driver

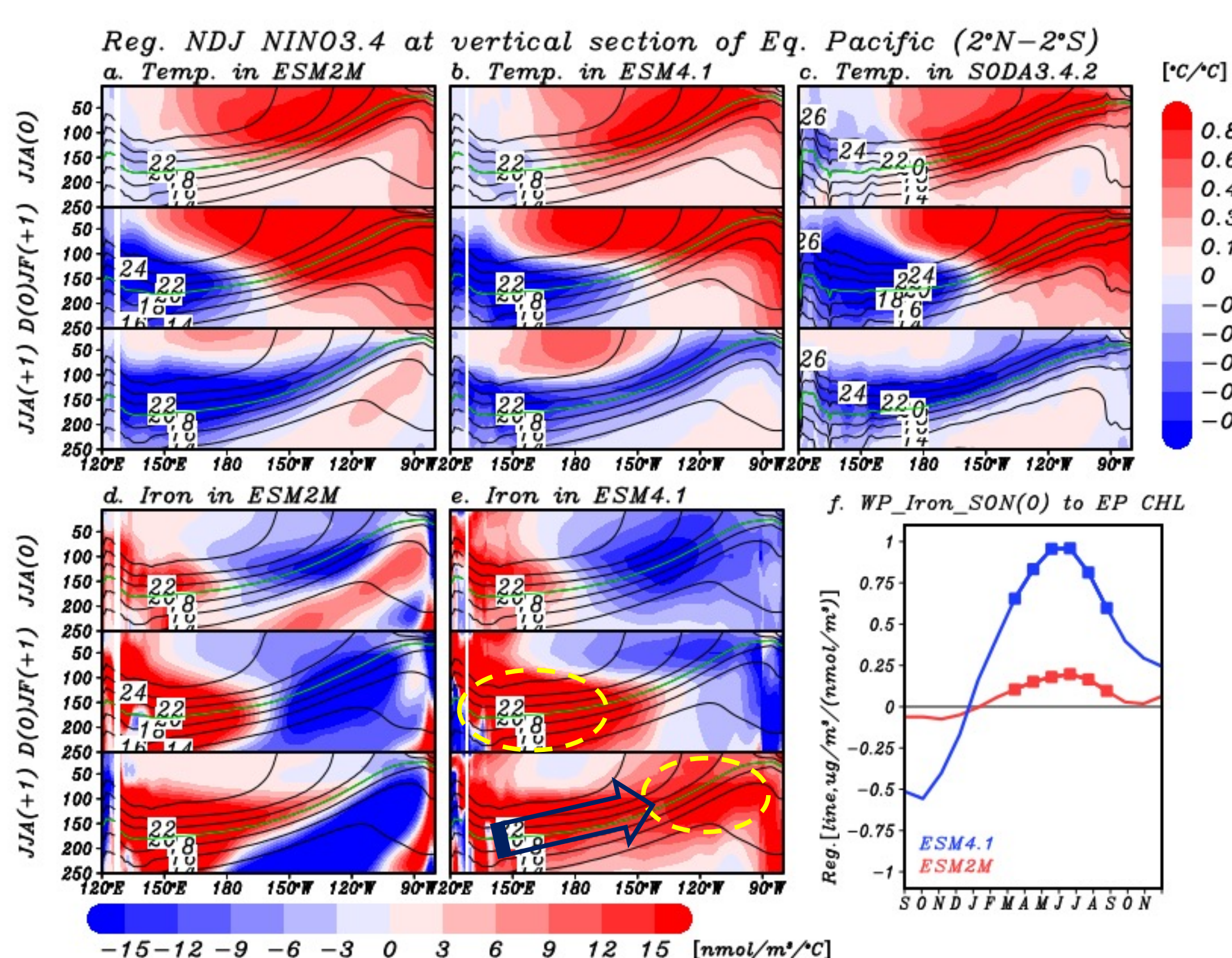


Figure 3. ENSO-regressed coefficients of vertical sections of equatorial temperature anomalies in (a) ESM2M, (b) ESM4.1, (c) SODA and dissolved iron concentration anomalies (shading) in (d) ESM2M, (e) ESM4.1. The temperature climatology from each model and SODA has been overlaid (contours) to aid interpretation and 20° C isotherm (green line) at equator (2° N– 2° S). (f) Regressed coefficients (square symbols denote the statistical significance at 95% confidence level) of iron concentration anomalies in the WP subsurface region averaged in ($130^\circ - 160^\circ$ E, 2° N– 2° S, 100–200 m depth) at SON(0) against the eastern EP surface ($160^\circ - 100^\circ$ W, 5° S– 5° N) monthly chlorophyll concentration anomalies simulated in ESM2M (red) and ESM4.1 (blue).

ENSO-CHL coupling in OBS, ESM2M, ESM4

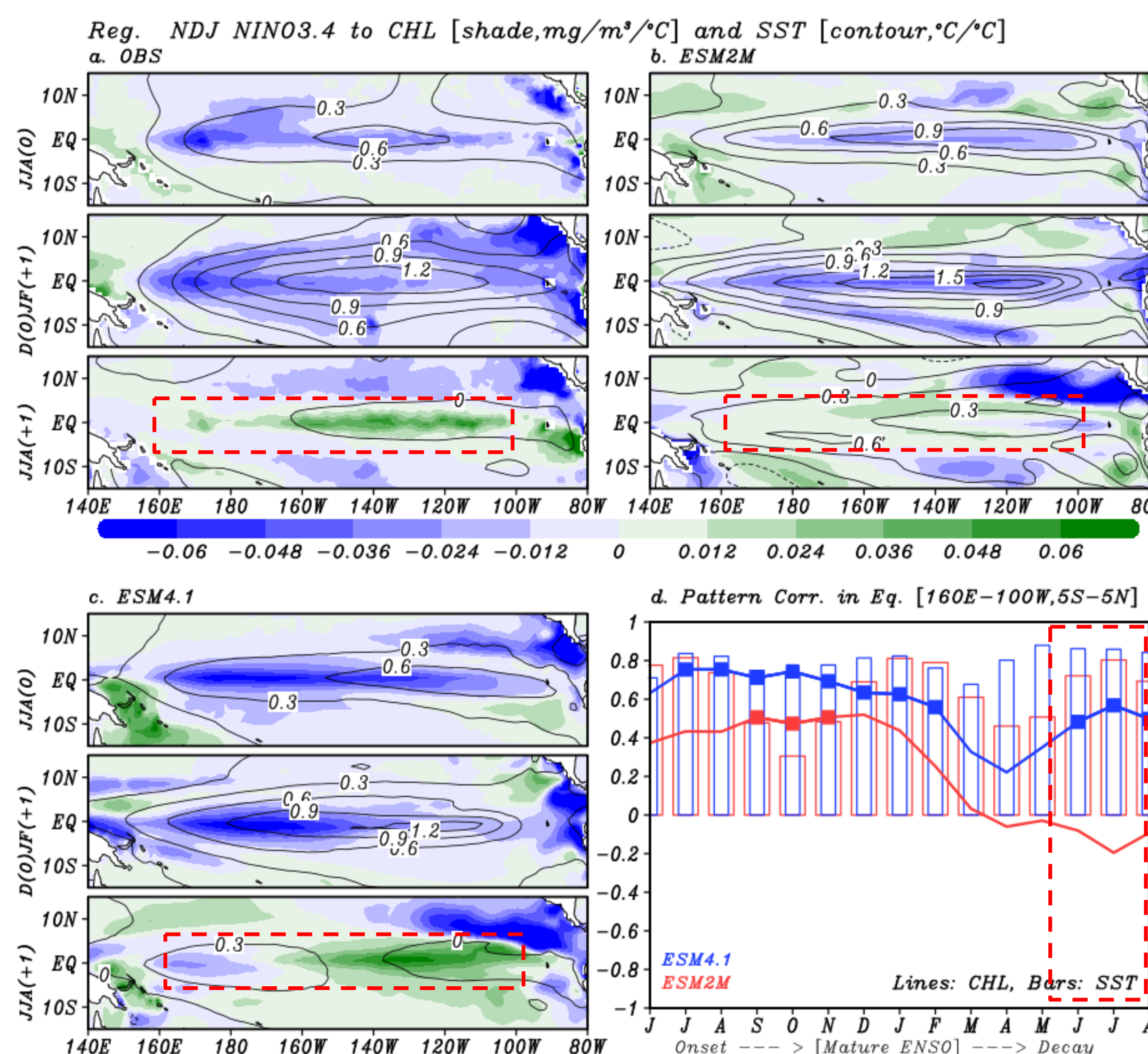


Figure 4. Spatially resolved ENSO-regression of temperature (contours, $^\circ$ C/ $^\circ$ C) and chlorophyll concentration (shading, $\text{mg}/\text{m}^3/^\circ$ C) anomalies against ENSO in (a) satellite, SODA, (b) ESM2M, and (c) ESM4.1. Values are shown for ENSO onset (JJA(0)), mature state (D(O)JF(+1)), and decay (JJA(+1)) ENSO states; (d) pattern correlations of ESM2M (red) and ESM4.1 (blue) regression coefficients (i.e., panels b and c) with SODA (bars) and satellite chlorophyll (lines); square symbols denote the Student's t-test statistical significance at 95% confidence level) regression coefficients (i.e., panel a) in the EP (160° E– 100° W, 5° N– 5° S).

Post El Niño Iron rebound

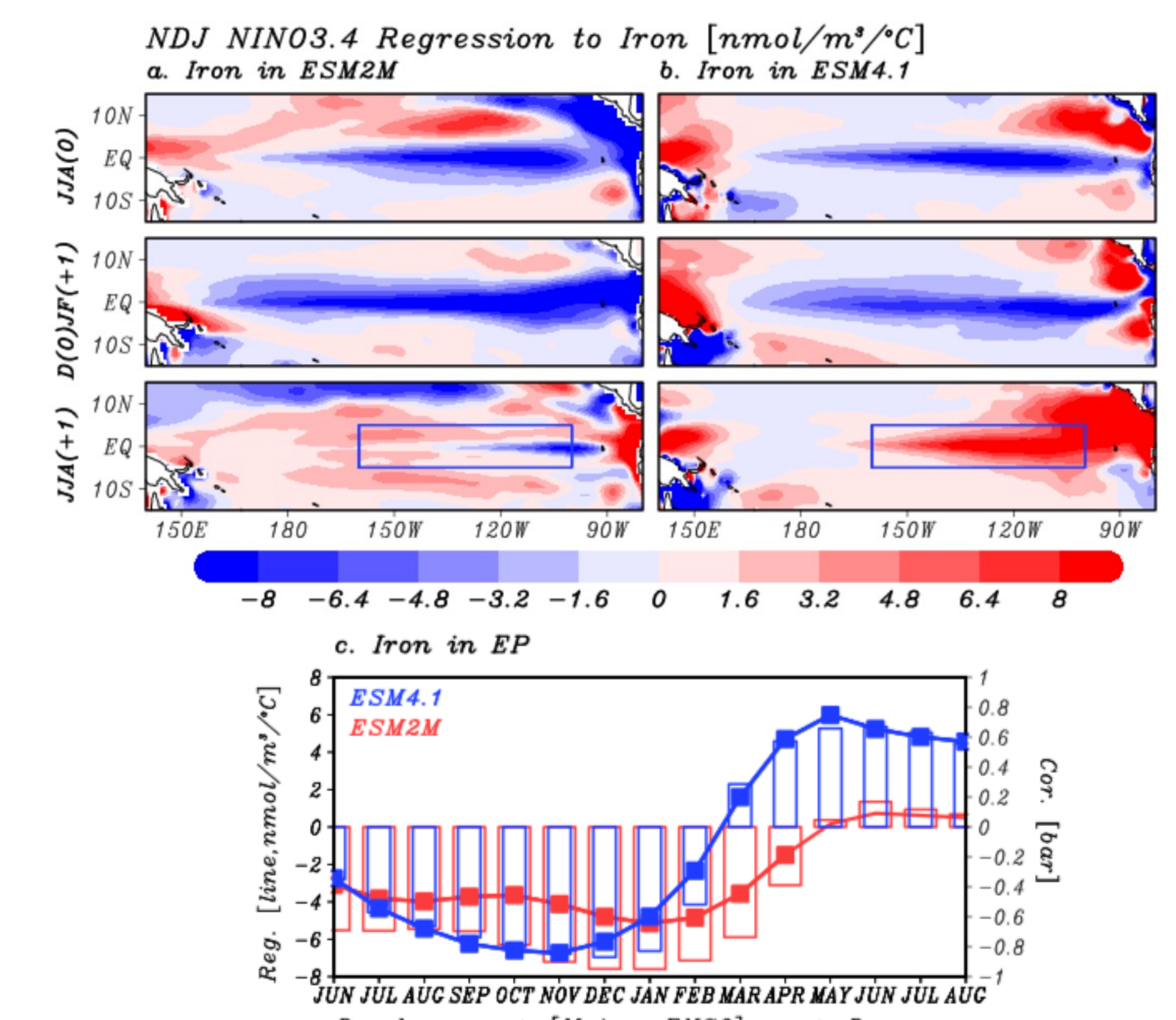


Figure 5. ENSO-regressed patterns in spatially resolved surface iron concentration anomalies ($\text{nmol}/\text{m}^3/^\circ$ C) in (a) ESM2M and (b) ESM4.1. (c) lead-lag ENSO regression (lines; square symbols denote the Student's t-test statistical significance at 95% confidence level) and correlation (bar) coefficients in regional monthly iron concentration anomalies in the eastern EP ($160^\circ - 100^\circ$ W, 5° S– 5° N).

Atmospheric Driver

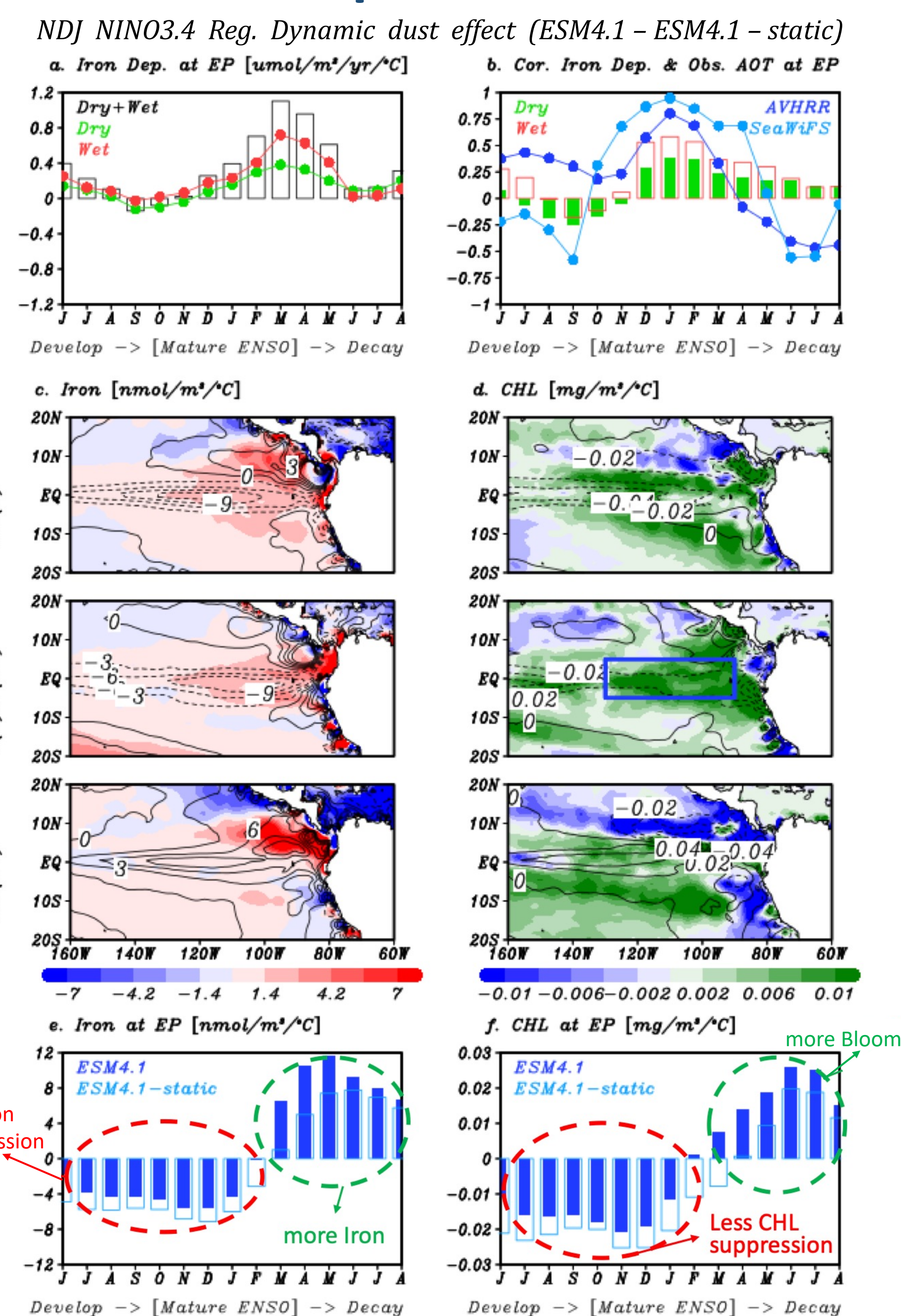
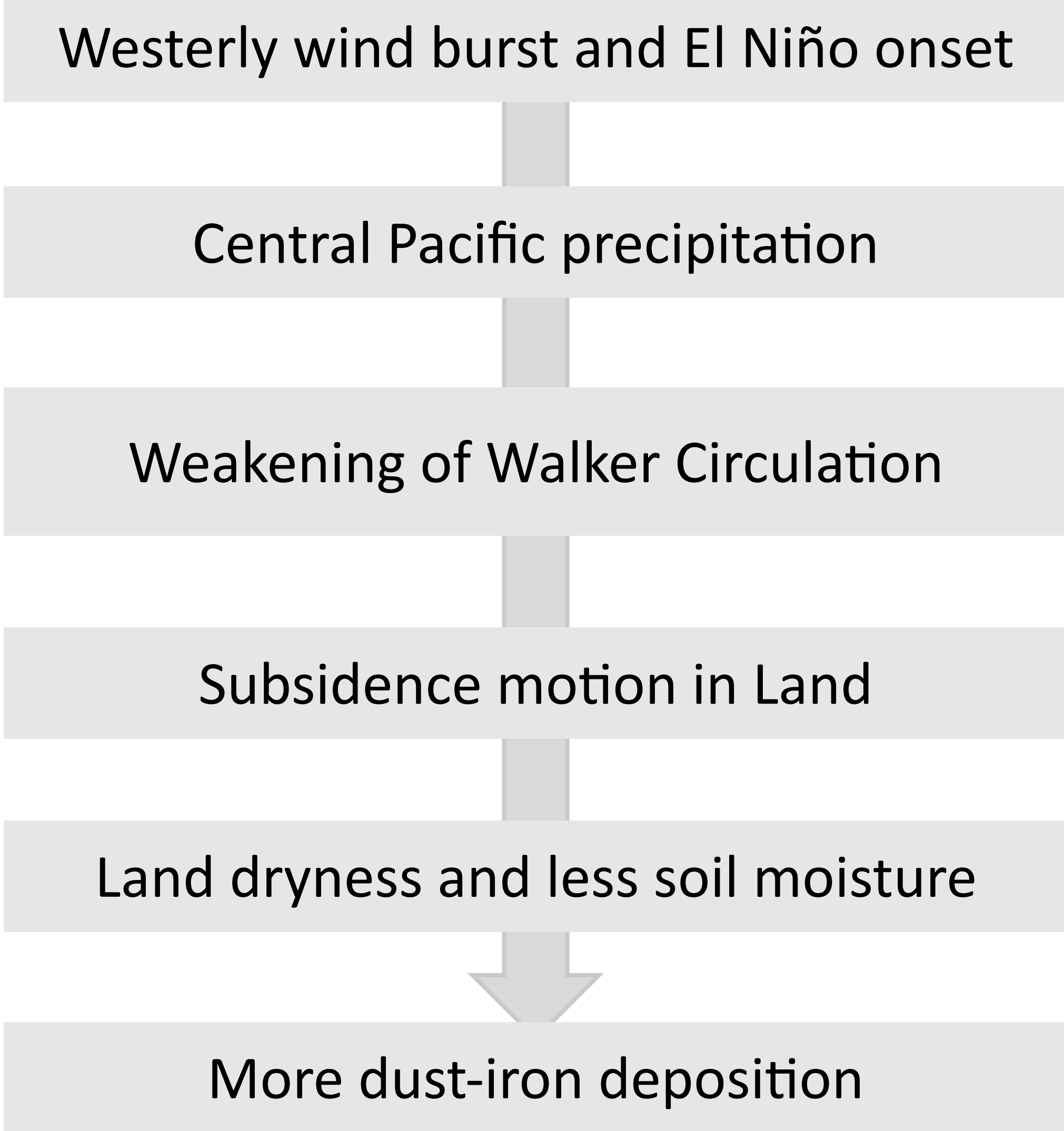


Figure 6. (a) ENSO-regression coefficient of dry (green), wet (red), and total (black bar) iron deposition ($\mu\text{mol}/\text{m}^2/\text{yr}/^\circ$ C) in ESM4.1 averaged in the eastern EP ($160^\circ - 100^\circ$ W, 5° S– 5° N). Panel (b) is the same as (a) but for correlation coefficients in dry (green bar) and wet (red bar) deposition anomalies in ESM4.1 and observed aerosol optical thicknesses (AOT) obtained from AVHRR (blue line) and SeaWiFS (sky blue line). Spatially resolved ENSO-regression coefficient differences (dynamic dust effects; shading) of (c) iron and (d) chlorophyll anomalies between ESM4.1 and ESM4.1-static; contours denote the ENSO-regression coefficient in iron and chlorophyll anomalies in ESM4.1-static. ENSO-regressed (e) iron and (f) chlorophyll anomalies averaged in the eastern EP in ESM4.1 (blue) and ESM4.1-static (sky blue).

Mechanism: El Niño to dust-iron



Conclusion

Better capturing post-El Niño CHL rebound pattern in GFDL-ESM4.1 (Fig. 1)

- **Much more iron supply** (Fig. 2) in post-El Niño event into the eastern equatorial Pacific in ESM4.1 than ESM2M
- ****Oceanic driver** (Fig. 3): Iron trapping and its propagation via equatorial undercurrent (Dominant factor to ENSO-CHL rebound)
- **Atmospheric driver** (Fig. 4): Less precipitation on land increases dust-iron deposition (Argument factor to ENSO-CHL sensitivity)
 - The chlorophyll rebound in GFDL-ESM4.1 may provide a key source of resilience to marine ecosystem simulation in the equatorial Pacific for management of living marine resources.

Further descriptions and references at:

Lim, H.-G., Dunne, J. P., Stock, C. A., Ginoux, P., John, J. G., & Krasting, J. (2022). *Oceanic and atmospheric drivers of post-El-Niño chlorophyll rebound in the equatorial Pacific*. *Geophysical Research Letters*, 49, e2021GL096113. <https://doi.org/10.1029/2021GL096113>